OPTICS

Full-color fluorescent carbon quantum dots

Liang Wang[1,2*†], Weitao Li[1*], Luqiao Yin[3], Yijian Liu[1], Huazhang Guo[1], Jiawei Lai[2], Yu Han[1], Gao Li[1], Ming Li[1], Jianhua Zhang[3], Robert Vajtai[2], Pulickel M. Ajayan[2], Minghong Wu[1†]

Quantum dots have innate advantages as the key component of optoelectronic devices. For white light–emitting diodes (WLEDs), the modulation of the spectrum and color of the device often involves various quantum dots of different emission wavelengths. Here, we fabricate a series of carbon quantum dots (CQDs) through a scalable acid reagent engineering strategy. The growing electron-withdrawing groups on the surface of CQDs that originated from acid reagents boost their photoluminescence wavelength red shift and raise their particle sizes, elucidating the quantum size effect. These CQDs emit bright and remarkably stable full-color fluorescence ranging from blue to red light and even white light. Full-color emissive polymer films and all types of high–color rendering index WLEDs are synthesized by mixing multiple kinds of CQDs in appropriate ratios. The universal electron-donating/withdrawing group engineering approach for synthesizing tunable emissive CQDs will facilitate the progress of carbon-based luminescent materials for manufacturing forward-looking films and devices.

INTRODUCTION

White light–emitting diodes (WLEDs) hold great promise for the next generation of ideal lighting devices in terms of their high energy efficiency, long lifetime, fast response speed, and high reliability (*1*). Nowadays, a combination of a blue or ultraviolet (UV) LED chip and multicolor phosphors are commonly used to generate white light (*2*). Much remarkable effort has been devoted to optimizing the properties of phosphors for their potential applications in WLEDs. A considerable number of fluorescent materials have been researched for their applications in WLEDs, including proteins (*3*), semiconductor quantum dots (QDs) (*4*–*6*), perovskite QDs (*7*, *8*), rare earth–based nanoparticles (*9*–*11*), polymers (*12*), metal complexes (*13*), and dyes (*14*). However, challenging synthesis, stability, and cytotoxicity of many materials still hinder their potential applications (*4*–*8*).

Nanoscale carbon QDs (CQDs) could fill this gap because of their biocompatibility, stability, and cost-effectiveness if these CQDs are made to fluoresce over a range of practically useful wavelengths (*15*–*19*). The inherent challenge in CQDs is the tunability of emission, as most of the CQDs are known to produce only blue, green, and yellow emissions (*20*–*22*). Supposing that the CQDs are capable of being prepared in a scalable fashion and their fluorescence is extended across the entire visible spectrum, the CQDs can work as excellent building blocks for all types of WLEDs. To this end, it is of paramount importance that optimum CQDs could be designed by choosing the right precursors and processing techniques. A few attempts have been achieved by using suitable precursors and complicated column chromatography postprocessing techniques in the past 5 years (*17*, *18*, *23*, *24*). Although the improved optical properties of these CQDs offered advantages in device performance, we note that no study has yet been reported that uses previously unidentified synthesis techniques. In pursuit of high–color rendering index (CRI > 80) WLEDs, especially the warm WLEDs, the robust CQDs with tunable photoluminescence (PL) emission will inevitably require a feasible approach involving the practical synthesis techniques.

Here, we report a novel one-step acid reagent engineering strategy to acquire highly luminescent CQDs, having remarkably tunable and stable fluorescence emission from blue to red and even white light by using *o*-phenylenediamine (oPD) as the precursor. The relative PL quantum yields (QYs) of these CQDs reached 72%. Our detailed studies prove that by controlling the acid reagents in reactions, we can readily modulate the particle size and fluorescence wavelength of CQDs over a wide range. To gain fundamental insights into the engineering mechanism of acid reagents, we analyzed the trend of electron-withdrawing and electron-donating groups on the surface of CQDs, of which the PL wavelengths and particle sizes of the CQDs are positively related to their amount of electron-withdrawing groups. Furthermore, the quantum size effect is elucidated. This work is the typical demonstration of the preparation of high-performance multicolor emissive CQDs through an electron-donating/withdrawing group engineering pathway without any complicated postprocessing. Full-color emissive polymethyl methacrylate (PMMA) films are also achieved by adding one or more types of these CQDs to the colloid mixtures. By adding CQDs into silica gel, we fabricate all kinds of high-CRI WLEDs, including warm, standard, and cool WLEDs, paving a way to practically applicable WLEDs. Our finding establishes a versatile technique for desirable optical properties of carbon and related zero-dimensional materials by electron-donating/withdrawing group engineering.

RESULTS

Synthetic strategy of full-color fluorescent CQDs

We demonstrated a one-step acid reagent engineering method for the synthesis of highly efficient full-color fluorescent CQDs by heating a mixture of oPD and selected acid reagents in ethanol solvent (Fig. 1A). Different acid reagents were chosen, and their fusion capability was evaluated in the preparation of CQDs under the same condition. The fluorescent properties of synthesized products were observed under UV light. Most of the as-prepared solutions only emitted blue and dim green fluorescence (fig. S1A) in that many acids are strong acids, which will easily cause excessive carbonization and defects during the reaction, resulting in weak optical properties of

[1]Institute of Nanochemistry and Nanobiology, School of Environmental and Chemical Engineering, Shanghai University, Shanghai 200444, P. R. China. [2]Department of Materials Science and NanoEngineering, Rice University, Houston, TX 77005, USA. [3]Key Laboratory of Advanced Display and System Applications, Ministry of Education, Shanghai University, Shanghai 200072, P. R. China.
*These authors contributed equally to this work.
†Corresponding author. Email: wangl@shu.edu.cn (L.W.); mhwu@shu.edu.cn (M.W.)

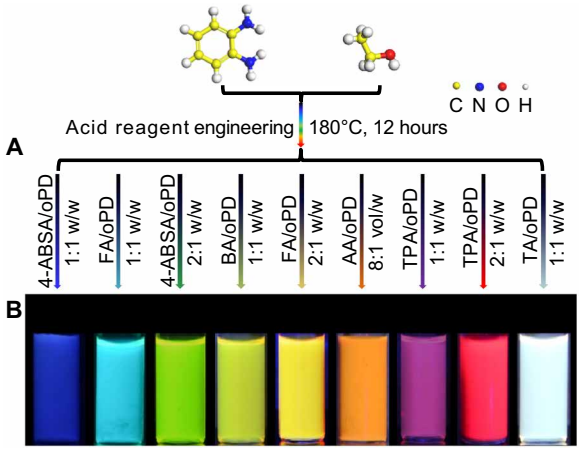

Fig. 1. Synthetic strategy of full-color fluorescent CQDs. (**A**) An acid reagent engineering strategy for the synthesis of full-color fluorescent CQDs using oPD as the precursor. (**B**) Fluorescence photographs of CQDs under UV light (excited at 365 nm).

CQDs. Other than these acids for fabricating CQDs, a few mild acids were used to modulate the optical properties of CQDs by means of adjusting the mass ratio between oPD and specific acid reagents [4-aminobenzenesulfonic acid (4-ABSA), folic acid (FA), boric acid (BA), acetic acid (AA), terephthalic acid (TPA), and tartaric acid (TA)] in solvothermal reactions (Fig. 1A). To eliminate the self-fluorescence impact of oPD or chosen acid to CQDs in the fusion step, subjecting pure oPD or acid reagents to the solvothermal reaction in ethanol just outputted blue-green fluorescence products (fig. S1B). When oPD met with an appropriate acid reagent, the synthesized CQDs emitted full-color fluorescence ranging from blue to red and even white light under UV light irradiation, manifesting tunable PL emission (Fig. 1B). The oPD constructs the structural skeleton of CQDs during the solvothermal treatment. In addition, the suitable acid is adopted to introduce different functional groups with various ratios into the structure of CQDs and to passivate the surface of CQDs, controlling particle sizes, reducing defects, and enhancing optical performance. When using different ideal acid reagents, six typical CQDs with blue, cyan, yellow-green, orange, red, and white fluorescence were created and labeled as b-CQDs, c-CQDs, yg-CQDs, o-CQDs, r-CQDs, and w-CQDs, respectively.

Structural and morphological characterizations

The compositions of the five typical CQDs (except w-CQDs) were analyzed by Fourier transform infrared (FTIR) spectra and x-ray photoelectron spectroscopy (XPS). All these CQDs contain the same four stretching vibration bands in their FTIR spectra, such as OH/NH at 3300 to 3470 cm^{-1}, carboxylic C═O at 1700 cm^{-1}, sp^2 C═C at 1462 cm^{-1}, and C—OH at 1224 cm^{-1}, evidencing that the five samples are always cofunctionalized by strong electron-donating groups (e.g., OH and NH_2) and weak electron-withdrawing COOH groups (fig. S2A), originating from ethanol/oPD and acid reagents, respectively. The stretching vibration band SO_3 at 1025 cm^{-1} is observed in the spectrum of b-CQDs, similar to surface-related B—O at 1344 cm^{-1} and B—C at 1032 cm^{-1} in the spectrum of yg-CQDs, confirming that the b-CQDs and yg-CQDs are additionally functionalized by medium electron-withdrawing SO_3H and B—O related groups (*25*), respectively. Nuclear magnetic resonance (NMR) spectroscopy (^{13}C and ^{1}H) was used to distinguish functional groups on the surface of CQDs (fig. S2, B and C). In their ^{13}C NMR spectra, the observed signals in the range of 100 to 150 parts per million (ppm) are assigned to sp^2 C (*15*, *26*). The active H signals from the NH_2 groups and aromatic hydrogen are detected in the range of 6 to 8 ppm in the ^{1}H NMR spectra, which further demonstrates the presence of electron-donating NH_2 groups on the surface of these CQDs. XPS findings were also carried out to investigate the surfaces of these samples (fig. S2, D to I) and to reconfirm the FTIR analysis results. All of the full spectra of five chosen samples show three typical peaks: C1s (285 eV), N1s (399 eV), and O1s (532 eV) (*27*). Besides, the spectra of b-CQDs and yg-CQDs show the S2p and B1s peaks, respectively, further corroborating the conclusion of the FTIR data. All of the C1s band of CQDs can be deconvoluted into three peaks, relevant to C═C/C—C (284.5 eV), C—N/C—O (286.1 eV), and carboxylic O—C═O (288.5 eV). Apart from that of yg-CQDs, there was a new peak (C—B, 283.4eV) (*25*). The whole N1s band displays the NH_2 groups (399.2 eV). All the O1s band of CQDs can be deconvoluted into two peaks of C═O (531.6 eV) and C—O (533.2 eV), respectively (*17*). The S2p band of b-CQDs is decomposed into two peaks at 163.5 and 167.4 eV, representing $SO_3/2P_{3/2}$ and $SO_3/2P_{1/2}$, respectively (*28*). The B1s band of yg-CQDs is divided into two peaks, corresponding to B—C (191.9 eV) and B—O (193.4 eV). The atomic ratio of the electron-donating NH_2 groups and carbon element decreases from 0.26 to 0.12 as the electron-donating OH group content declines from b-CQDs to r-CQDs (table S1), which has a similar decreasing tendency of the atomic ratio of NH_2 and carbon in the elemental analysis (table S1). In contrast, the amount of electron-withdrawing COOH groups notable increase from 45.51% (b-CQDs) to 71.64% (r-CQDs), reflecting that the increasing electron-withdrawing groups, derived from acid reagents and grafted on the surface of these CQDs, can boost the PL wavelength red shift of the CQDs. Furthermore, increasing the ratio of the same acid reagent in the fusion process, such as 4-ABSA, FA, and TPA (Fig. 1B), also reveals the PL wavelength red shift phenomenon of the CQDs, illustrating the spectral engineering role of acid reagents in the solvothermal reaction.

The morphology of these samples was observed by transmission electron microscopy (TEM) and atomic force microscopy (AFM). The TEM images exhibit that these CQDs are uniform and monodispersed nanodots in Fig. 2 (A to E). Their average lateral sizes are about 1.71, 1.83, 1.95, 2.2, and 2.42 nm for b-CQDs, c-CQDs, yg-CQDs, o-CQDs, and r-CQDs, respectively. The high-resolution TEM images illustrate the high crystallinity structure of CQDs with similar well-resolved lattice fringes. The crystal plane spacing of 0.21 nm corresponds to the (100) graphite plane (Fig. 2, F to J) (*29*). The average heights of the CQDs range from 0.48 to 0.66 nm in Fig. 2 (K to O), elucidating that they consist of one to two layers of graphite (*30*). The x-ray diffraction (XRD) patterns indicate a distinct peak at around 25.3°, signifying a nearly identical (002) layer spacing of the CQDs (fig. S2J) (*31*). Layer spacing (3.78 Å) in the b-CQDs functionalized by SO_3 is substantially more extensive than that of other CQDs (3.31 to 3.57 Å), which is demonstrated in our previous work (*28*). Their graphitic structure is reflected in Raman spectra. The intensity ratios of the crystalline G band at 1520.8 cm^{-1} and disordered D band at 1381.8 cm^{-1} (I_G/I_D) are 0.93, 1.04, 1.14, 1.17, and 1.38 from b-CQDs to r-CQDs, respectively (fig. S2K). The increasing ratio values imply the strengthened graphitization degree from b-CQDs to r-CQDs, indicating a gradual increase of the size of sp^2 domains

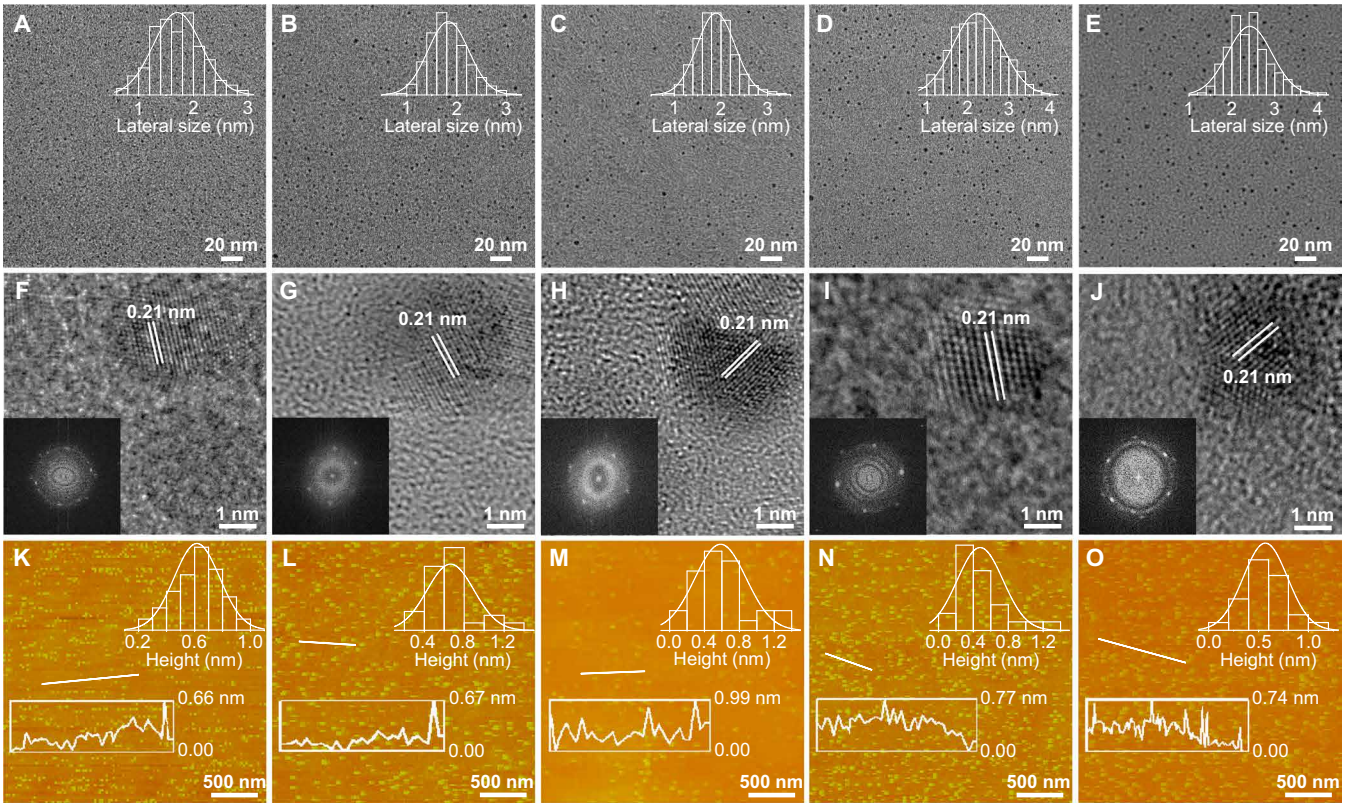

Fig. 2. Morphological characterizations of selected CQDs. (**A** to **E**) TEM images and corresponding lateral size distributions of b-CQDs (A), c-CQDs (B), yg-CQDs (C), o-CQDs (D), and r-CQDs (E). (**F** to **J**) High-resolution TEM images of b-CQDs (F), c-CQDs (G), yg-CQDs (H), o-CQDs (I), and r-CQDs (J) (inset: fast Fourier transform patterns). (**K** to **O**) AFM images and corresponding height profiles of b-CQDs (K), c-CQDs (L), yg-CQDs (M), o-CQDs (N), and r-CQDs (O).

(*17*, *32*), which is consistent with the above TEM results. These consequents provide essential progress toward the understanding of the engineering role of acid reagents in the realization of highly efficient full-color CQDs. The acid reagents introduce electron-withdrawing groups on the surface of CQDs, which are performed to effectively modulate the degree of graphitization, and thereby construct their increasing particle size with red shift tunable emission.

Optical performance

To gain the optimal optical features of CQDs, we modulated their QYs by adjusting the acid reagent concentration and temperature of the reaction (fig. S3, A to J). The optimal QYs for the CQDs are deemed to range from 25 to 72% (table S2), overstepping majority CQDs reported to date (*33*–*35*). The yg-CQDs with the highest QYs among these CQDs demonstrate similar fluorescent properties with rhodamine 6G (a commonly used reference for measuring QYs) (fig. S3K). As shown in Fig. 3A, the absorption spectra of the CQDs exhibit strong excitonic absorption bands at 377, 428, 454, 571, and 628 nm for b-CQDs, c-CQDs, yg-CQDs, o-CQDs, and r-CQDs, respectively, which is similar to the absorption characteristics of traditional semiconductor QDs and unlike previously reported CQDs within the UV region (*25*, *26*). The normalized PL spectra of CQDs also display PL peaks at about 450 nm (b-CQDs), 490 nm (c-CQDs), 540 nm (yg-CQDs), 600 nm (o-CQDs), and 665 nm (r-CQDs), respectively (Fig. 3B). We tested various solvents to investigate the solvation effect in the fabrication process of the CQDs. In comparison with the CQDs manufactured in ethanol, the excitonic absorption bands of most of these CQDs synthesized in water, *N*,*N*′-dimethylformamide (DMF), and toluene are inhibited within 500 nm (fig. S1, C to H) and do not show the wide spectral response characteristic like full-color CQDs. Meanwhile, the modulation of their PL peaks only ranges from 420 to 610 nm, which is limited compared with the optical properties of CQDs fabricated in ethanol. The optical phenomenon of CQDs produced in various solvents suggests that the reaction solution with high or low polarity led to a notable blue shift of optical properties of CQDs and illustrates that medium polarity ethanol is the most advisable solvent to synthesize CQDs with the desired optical properties. Notably, the CQDs demonstrate excitation-independent PL emissions (fig. S4, A to E) due to their highly ordered graphitic structure (fig. S2K) (*27*). The maximum PL excitation peak is centered at 355 nm (b-CQDs), 410 nm (c-CQDs), 440 nm (yg-CQDs), 535 nm (o-CQDs), and 600 nm (r-CQDs), respectively (fig. S4F), which is consistent with the relevant excitonic absorption band (fig. S4G), revealing the band-edge emission properties of CQDs (*15*, *36*). Meanwhile, the gradual increase of CQD size from 1.7 to 2.4 nm agrees with the corresponding PL wavelength and the first excitonic absorption band (Fig. 3C), elucidating the quantum size effect (*15*, *17*, *27*–*29*, *37*). Moreover, the time-resolved PL spectra, illustrating the band-edge emission properties of CQDs, were further measured. A decreasing trend of monoexponential lifetimes of the CQDs from 10.91 ns (b-CQDs) to 2.49 ns (r-CQDs) (Fig. 3D and table S3) indicates that the CQDs' lifetime decreases with their PL wavelength red shift (*15*). Furthermore, these CQDs retain the long-term photostability (>10 hours) under UV light irradiation

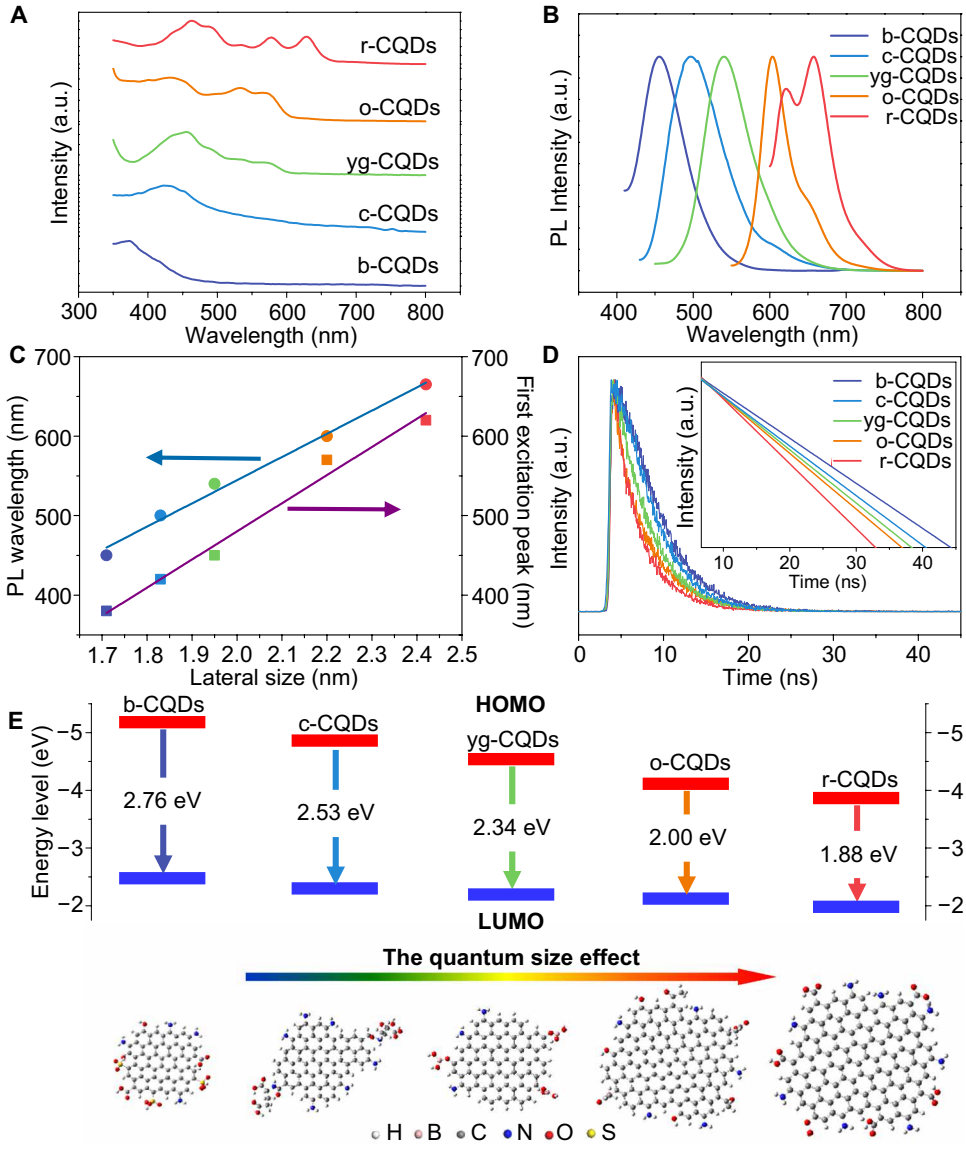

Fig. 3. Optical performance of selected CQDs. (**A**) Absorption spectra of CQDs. (**B**) Normalized PL spectra of CQDs. (**C**) Dependence of the PL wavelength and first excitonic absorption band on the particle size of CQDs. (**D**) Time-resolved PL spectra of CQDs. (**E**) Dependence of the HOMO and LUMO energy levels concerning the particle size of CQDs. a.u., arbitrary units.

and good temperature tolerance (fig. S4, H to Q), which is a benefit for long-term observation of the CQD-based technological devices. As a consequence, the QYs of these CQDs are markedly improved by optimizing reaction conditions. Besides, these CQDs have unique tunable fluorescence properties. Accompanied by the excellent photostability and thermal stability, these CQDs will generally be applicable for advanced WLEDs.

Bandgap energies of CQDs were calculated using the equation $E_g^{opt} = 1240/\lambda_{edge}$, where λ_{edge} is the wavelength of the maximum absorption edge. The calculated bandgap energies gradually decrease from 2.76 to 1.88 eV with the rising particle size of CQDs (table S3), further certifying the quantum size effect of CQDs. Meanwhile, the highest occupied molecular orbital (HOMO) energy level is determined by UV photoelectron spectroscopy, and the lowest unoccupied molecular orbital (LUMO) is gained on the basis of the optical bandgap energy and the HOMO energy level (fig. S5, A to E, and table S3). As seen from the energy diagram in Fig. 3E, there are similarly decreased trendies of HOMO and LUMO levels ranging from 5.22 to 3.83 eV and from 2.46 to 1.95 eV (the difference between energy gap and HOMO level), respectively, directly elucidating the interband transitions in the CQDs (fig. S5F and table S3) (*18*).

Unique w-CQDs

The w-CQDs have recently emerged as a candidate for innovative white luminescent materials for the replacement of present-day materials (*38*, *39*). Note that anchoring the w-CQD phosphor on the UV chip can directly fabricate WLEDs without further proportional control. However, all of the reported w-CQDs were obtained by strong acid activation of bulk carbon materials, which broke their intrinsic

sp^2-hybridized structure, created massive defects, and resulted in their weak white fluorescence (*39*, *40*). Thus, there is still a long way to get high-quality w-CQDs. Besides the multicolor CQDs, the high-performance w-CQDs were synthesized in an analogous route successfully. The w-CQDs emit bright white fluorescence when irradiated by UV light, obtaining the highest QY of 39% in all of the published w-CQDs (Fig. 4A) (*38*–*40*). The optical spectrum of w-CQDs demonstrates a broad PL ranging from 360 to about 800 nm (Fig. 4B), covering the entire visible light region. The wide full width at half maximum of w-CQDs is 208 nm, which is broader than that of the reported w-CQDs (*38*–*40*). Besides, w-CQDs also maintain an excellent photostability for 10 hours and thermal stability (fig. S6, A and B). Furthermore, the w-CQDs exhibit a monoexponential fluorescence lifetime of 3.07 ns in Fig. 4C. A graphitic structure with a (002) layer spacing is shown in the XRD pattern (fig. S6C), which closely resembled that of other selected CQDs. The large G-to-D intensity ratio of 1.36 verifies the high-ordered graphitization structure (fig. S6D). As shown in the FTIR spectrum of w-CQDs (fig. S6E), there are four sharp peaks ascribed to the NH_2, COOH, and OH groups on the surface of w-CQDs. The w-CQDs have the three-elemental composition (i.e., C, N, and O) in the XPS spectra (fig. S6, F to I). There is a C—N/C—O signal at 286.1 eV in the C1s spectrum and a strong signal of NH_2 to 399.2 eV in the N1s spectrum, indicating the existence of NH_2 groups. Similarly, the O1s spectrum reveals the presence of C═O at 531.6 eV and C—O at 533.2 eV, while the C═O signal at 288.6 eV is seen in the C1s spectrum. The XPS analysis further confirms the results of FTIR. The TEM image (Fig. 4D) reveals that the w-CQDs are well dispersed with an average lateral size of 3.01 nm. The high-resolution TEM image of w-CQDs shows well-resolved lattice fringes that resemble other selected CQDs (Fig. 4E). An average thickness of w-CQDs characterized by AFM (Fig. 4F) is 0.64 nm, also revealing an average layer number of ~1 to 2. There is no doubt that such superior w-CQDs are going to create highly efficient WLEDs soon.

Advanced WLED applications

The CQDs with unique optical properties could be used in several applications, such as full-color emissive films. The pure CQDs and mixtures with varying ratios of CQDs were applied to prepare full-color PMMA nanocomposite films (Fig. 5A and fig. S7A). All the obtained films are uniform and transparent (fig. S7A). These films indicate a broad range of PL emission colors under UV light at 365 nm in Fig. 5A. Except for a white light emission film (xvi) using pure w-CQDs, it is noted that two white luminous films (xiv and xv) could also be achieved with varying ratios of CQDs. Next, all types of WLEDs were fabricated by using CQDs in silica gel in various concentrations and mixtures, including warm WLED (I), standard WLED (II), and cool WLED (III) [inset in Fig. 5 (B to D)]. The warm WLED with low correlated color temperature (CCT < 4000 K) is strongly desired for indoor lighting because it makes our eyes relaxed and comfortable. However, it is difficult to improve its CRI over 80 because of a lack of efficient orange or red luminescent CQD-based phosphors (*16*). Here, the warm WLED made use of pure o-CQDs, as phosphor emits bright warm white light with CCT of 3913 K, Commission Internationale de L'Eclairage (CIE) color coordinate of (0.39, 0.38), and high CRI of 89.3 (Fig. 5B). When pure w-CQDs serve as the phosphor, a standard WLED with a CIE color coordinate of (0.33, 0.33) is acquired (Fig. 5C). The CCT and CRI of the WLED are 5994 K and as high as 86.7, respectively, and the emitted white light is very close to natural sunlight. By combining the b-CQDs, yg-CQDs, and r-CQDs with a weight ratio of 1:2:3, a cool WLED with the CIE color coordinate approaching (0.28, 0.29) and high-CRI (86.7) has also been achieved (Fig. 5D). The light-emitting spectrum of the WLEDs is shown in Fig. 5 (E to G), which also covers the whole visible light

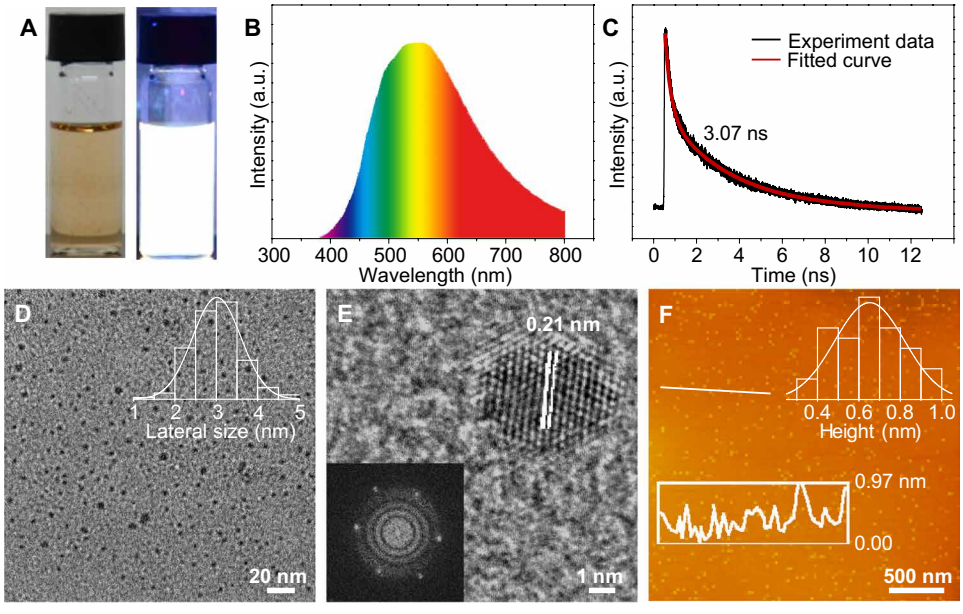

Fig. 4. Optical and morphological characterizations of w-CQDs. (**A**) Photographs of w-CQDs under daylight (left) and UV light (right) (excited at 365 nm). (**B**) PL spectrum of w-CQDs. (**C**) Time-resolved PL spectrum of w-CQDs. (**D**) TEM image and corresponding lateral size distribution of w-CQDs. (**E**) High-resolution TEM image and fast Fourier transform pattern of w-CQDs. (**F**) AFM image and corresponding height profile of w-CQDs.

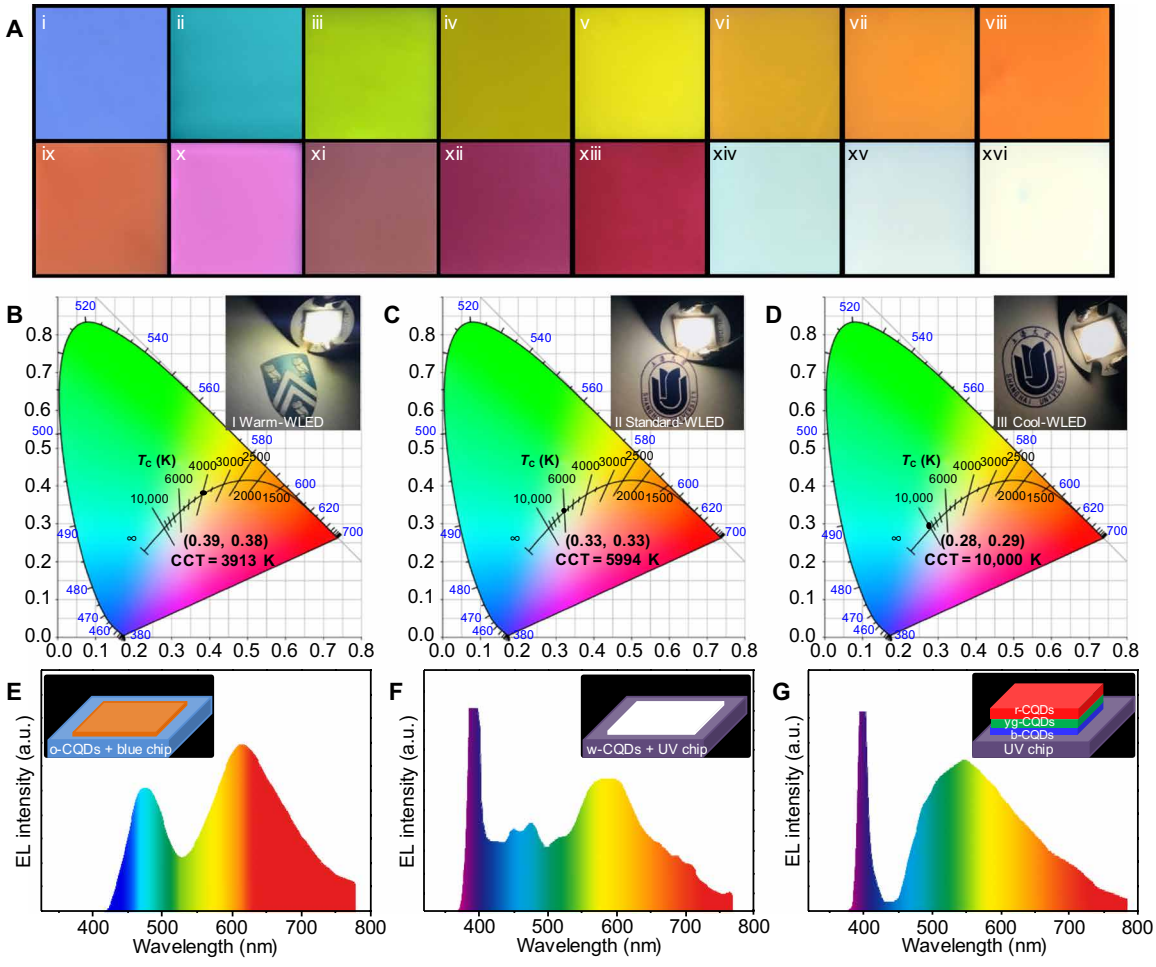

Fig. 5. Applications of full-color CQDs. (**A**) Fluorescence images of CQDs/PMMA composite films on glass substrates under UV light. (i) b-CQDs, (ii) c-CQDs, (iii) g-CQDs, (iv) y-CQDs/g-CQDs = 1:1, (v) yg-CQDs, (vi) y-CQDs, (vii) g-CQDs/o-CQDs = 1:1, (viii) o-CQDs, (ix) yg-CQDs/o-CQDs = 1:1, (x) r-CQDs/dr-CQDs = 1:1, (xi) dr-CQDs/b-CQDs = 1:1, (xii) r-CQDs, (xiii) dr-CQDs, (xiv) b-CQDs/yg-CQDs/dr-CQDs = 1:2:3, (xv) c-CQDs/y-CQDs/r-CQDs = 1:2:1, and (xvi) w-CQDs (all ratio scale w/w). (**B** and **E**) The CIE chromaticity coordinate and corresponding emission spectrum of the warm WLED (inset: the photograph and schematic of the warm WLED). (**C** and **F**) The CIE chromaticity coordinate and corresponding emission spectrum of the standard WLED (inset: the photograph and schematic of the standard WLED). (**D** and **G**) The CIE chromaticity coordinate and corresponding emission spectrum of the cool WLED (inset: the photograph and schematic of the cool WLED).

region from 400 to 780 nm. There are two visible PL peaks centered at about 475 and 620 nm in the light-emitting spectrum of warm WLED, whereas there is only a single PL peak near 600 and 550 nm for standard and cool WLED, respectively. Wholly, the full-color phosphors based on CQDs are promising candidates for practical display and all types of high-CRI WLED applications.

DISCUSSION

Although CQDs have inherent advantages of tunable PL emission for WLEDs, the CQD-based devices have traditionally encountered from both relatively low CRI and unimplemented all types of ideal WLEDs. Exploiting the practical synthesis techniques of advanced full-color CQDs is the ultimate vital implication for further success in WLED applications. In summary, we have successfully demonstrated a facile acid reagent engineering approach to manipulate highly efficient full-color tunable fluorescent emission CQDs. More specifically, the QYs of these CQDs are remarkably improved up to 72%. The synthesis strategy relies on the introduced acid reagents in the fusion process, which markedly plays a role in modulating PL phenomena of as-produced CQDs. The fluorescence emission of these CQDs can be tuned from blue to red and even white light. The maximum PL excitation peaks are consistent with the relevant excitonic absorption bands, and the lifetimes of the CQDs decrease with their PL wavelength red shift, also revealing the band-edge emission properties of CQDs. Moreover, the linear behavior between the particle size of CQDs and the corresponding PL wavelength illustrates the quantum size effect of as-prepared CQDs. In this way, the superiorities of the CQDs in high QYs, optical tunability, remarkable photostability, and thermal stability are perfectly integrated to build advanced WLED architectures. Eventually, by adding one or more types of these CQDs in appropriate ratios to the colloid mixtures, we have succeeded in fabricating the full-color luminous films and all types of WLED devices, including warm, standard, and cool WLEDs. The values of their CIE color coordinate are precisely located on the white light trajectory, and these WLEDs also exhibit higher CRI than 80. Furthermore, the CQDs display an excellent cell imaging ability with a good biocompatibility (fig. S7, B to F), which opens a highly exciting

scenario for the exploration of the advanced optoelectronic devices and future high-resolution bioimaging applications.

To elucidate the nature of the engineering role of acid reagents in the fusion process, we further pursued the functional groups on the surface of these CQDs via XPS and elemental analysis. With the illustration of XPS and elemental analysis evolutions, it reveals that introducing and increasing electron-withdrawing groups on the surface of CQDs mainly contribute to the rising particle sizes and PL wavelength red shift of the CQDs. Our approach discovered in this work constitutes a valuable proof of concept on the general electron-donating/withdrawing group engineering route for developing practical synthesis techniques of high-quality CQDs with tunable optical properties. The concept affirms killing three birds with one stone [i.e., (i) modulating particle size, (ii) tuning color emission, and (iii) realizing the advanced performance of CQD-based WLEDs]. Our findings may cause considerable repercussions to generate brand new envisages of processing techniques for advanced CQDs and other luminescent materials. We will attempt more systems to verify our discovery in the near future.

MATERIALS AND METHODS

Chemicals and materials

Reagent grades of oPD were purchased from Adamas. Ethanol, DMF, toluene, acids, and PMMA were provided by Sinopharm Chemical Reagent Co. Ltd. (Shanghai, China). All chemical reagents were used as received without further purification. Deionized water was used for all experiments.

Synthesis of full-color CQDs

The tunable fluorescent CQDs from blue to red and even white were prepared via a one-pot solvothermal process using acids and oPD as engineering reagents and the precursor. The CQDs from left to right in Fig. 1 were labeled as b-CQDs, c-CQDs, g-CQDs, yg-CQDs, y-CQDs, o-CQDs, r-CQDs, dr-CQDs, and w-CQDs, respectively. For b-CQDs and g-CQDs, oPD (0.1 g) and 4-ABSA (0.1 and 0.2 g) were dissolved in 10-ml ethanol solution. Afterward, the solution was transferred into a 25-ml Teflon-lined stainless steel autoclave and heated at 180°C for 12 hours for b-CQDs and g-CQDs, respectively. When the reaction temperature dropped to room temperature, the resulting solution was filtered with a 0.22-μm microporous membrane and then purified by dialysis in ethanol solvent. Last, the CQD powder could be obtained for further characterization after drying at 60°C. Other CQDs were prepared using a procedure similar to that described above for b-CQDs and g-CQDs, except for the different acids with suitable amount. Generally, the 0.05- and 0.1-g FA was used to react with oPD (0.05 g) for c-CQDs and y-CQDs, respectively. The 0.1-g BA was used to react with oPD (0.1 g) for yg-CQDs. The 0.8-ml AA was used to react with oPD (0.1 g) for o-CQDs. The 0.1- and 0.2-g TPA was used to react with oPD (0.1 g) for r-CQDs and dr-CQDs, respectively. The 0.1-g TA was used to react with oPD (0.1 g) for w-CQDs.

Preparation of full-color emissive films

For the blue/cyan/green/yellow-green/yellow/orange/magenta/red/white fluorescent glass films, 2 ml of the corresponding CQD solvent (5 mg·ml^{-1}) was mixed with 10 ml of PMMA solvent (10 mg·ml^{-1}), then dropped on a cleaned glass sheet using spin-coating method, and dried for 1 day under ambient conditions. Among them, the mixed glass films are obtained with the corresponding weight ratio: (i) b-CQDs, (ii) c-CQDs, (iii) g-CQDs, (iv) y-CQDs/g-CQDs = 1:1, (v) yg-CQDs, (vi) y-CQDs, (vii) g-CQDs/o-CQDs = 1:1, (viii) o-CQDs, (ix) yg-CQDs/o-CQDs = 1:1, (x) r-CQDs/dr-CQDs = 1:1, (xi) dr-CQDs/b-CQDs = 1:1, (xii) r-CQDs, (xiii) dr-CQDs, (xiv) b-CQDs/yg-CQDs/dr-CQDs = 1:2:3, (xv) c-CQDs/y-CQDs/r-CQDs = 1:2:1, and (xvi) w-CQDs (all ratio scale w/w).

Fabrication of WLEDs

Warm WLED was fabricated with the o-CQDs and a blue LED chip. Standard and cool WLEDs were manipulated with the w-CQDs, mixed CQDs with the appropriate weight ratio (b-CQDs/yg-CQDs/r-CQDs = 1:2:1), and a UV LED chip, respectively. All types of WLEDs have a similar preparation process. The CQDs (5 mg) were added to 1.6 g of ET-821A silica gel and 0.4 g of ET-821B silica gel. Then, the mixture was stirred for 15 min (50 rpm) and added dropwise to a blue or UV LED chip, respectively. Then, the device was dried in an oven at 50°C for 30 min.

Material characterization

The photographs were taken with a camera (Nikon D7000) under UV light excited at 365 nm (6000 μW·cm^{-2}; S4020-6K). AFM images were characterized using an SPM-9600 AFM. TEM observations were performed on aberration-corrected TEM (JEM-2100F) operating at 80-kV acceleration voltage. FTIR spectra of dried samples were recognized with a Bio-Rad FTIR spectrometer FTS165. XPS spectra were gathered using a Kratos Axis Ultra DLD x-ray photoelectron spectrometer. Elemental analysis was performed on vario MICRO. ^{1}H NMR and ^{13}C NMR spectroscopy were carried out with JEOL resonance ECZ400S 400-MHz spectrometer using dimethyl sulfoxide–D6 as the solvent. XRD patterns were obtained with a Rigaku 18 KW D/max-2550 using Cu K_α radiation. Raman spectra were recorded on a Thermo Fisher Scientific DXRxi laser Raman spectrometer with λ_{ex} = 633 nm. Absorption and fluorescence spectra were registered at room temperature on a Hitachi 3010 spectrophotometer and a Hitachi 7000 fluorescence spectrophotometer. The time-resolved PL spectra were measured on an Edinburgh FS5 spectrofluorometer. The PL QY of CQD solutions was determined by comparing the integrated PL intensities and the absorbency values using rhodamine 6G in water (QY: 95%) as the reference. The UV photoelectron spectroscopy was measured with a monochromatic He I light source (21.22 eV; ESCALAB 250XI, Thermo Fisher Scientific) and a VG Scienta R4000 analyzer. A sample bias of −5 V was applied to observe the secondary electron cutoff. The work function (ϕ) can be determined by the difference between the photon energy and the binding energy of the secondary cutoff edge. The CQD thin film was prepared from spin-coating on the indium tin oxide substrate for UV photoelectron spectroscopy measurement. The photoelectric properties, including the emission spectra, CCT, CRI, and CIE color coordinates of the WLEDs, were measured by using a high-accuracy array spectroradiometer (HAAS-2000, Everfine).

SUPPLEMENTARY MATERIALS

Supplementary material for this article is available at http://advances.sciencemag.org/cgi/content/full/6/40/eabb6772/DC1

REFERENCES AND NOTES

1. A. L. Chun, E. De Ranieri, A. Moscatelli, O. Vaughan, Our choice from the recent literature. *Nat. Nanotechnol.* **10**, 568 (2015).
2. G. Li, Y. Tian, Y. Zhao, J. Lin, Recent progress in luminescence tuning of Ce^{3+} and Eu^{2+}-activated phosphors for pc-WLEDs. *Chem. Soc. Rev.* **44**, 8688–8713 (2015).

3. M. D. Weber, L. Niklaus, M. Pröschel, P. B. Coto, U. Sonnewald, R. D. Costa, Bioinspired hybrid white light-emitting diodes. *Adv. Mater.* **27**, 5493–5498 (2015).
4. A. Lita, A. L. Washington II, L. van de Burgt, G. F. Strouse, A. E. Stiegman, Stable efficient solid-state white-light-emitting phosphor with a high scotopic/photopic ratio fabricated from fused CdSe-silica nanocomposites. *Adv. Mater.* **22**, 3987–3991 (2010).
5. E. Jang, S. Jun, H. Jang, J. Lim, B. Kim, Y. Kim, White-light-emitting diodes with quantum dot color converters for display backlights. *Adv. Mater.* **22**, 3076–3080 (2010).
6. B. Xie, H. Liu, R. Hu, C. Wang, J. Hao, K. Wang, X. Luo, Targeting cooling for quantum dots in white QDs-LEDs by hexagonal boron nitride platelets with electrostatic bonding. *Adv. Funct. Mater.* **28**, 1801407 (2018).
7. G. Li, H. Wang, T. Zhang, L. Mi, Y. Zhang, Z. Zhang, W. Zhang, Y. Jiang, Solvent-polarity-engineered controllable synthesis of highly fluorescent cesium lead halide perovskite quantum dots and their use in white light-emitting diodes. *Adv. Funct. Mater.* **26**, 8478–8486 (2016).
8. C. Sun, Y. Zhang, C. Ruan, C. Yin, X. Wang, Y. Wang, W. W. Yu, Efficient and stable white LEDs with silica-coated inorganic perovskite quantum dots. *Adv. Mater.* **28**, 10088–10094 (2016).
9. H. Daicho, T. Iwasaki, K. Enomoto, Y. Sasaki, Y. Maeno, Y. Shinomiya, S. Aoyagi, E. Nishibori, M. Sakata, H. Sawa, S. Matsuishi, H. Hosono, A novel phosphor for glareless white light-emitting diodes. *Nat. Commun.* **3**, 1132 (2012).
10. W. B. Im, N. George, J. Kurzman, S. Brinkley, A. Mikhailovsky, J. Hu, B. F. Chmelka, S. P. DenBaars, R. Seshadri, Efficient and color-tunable oxyfluoride solid solution phosphors for solid-state white lighting. *Adv. Mater.* **23**, 2300–2305 (2011).
11. Y. H. Kim, P. Arunkumar, B. Y. Kim, S. Unithrattil, E. Kim, S.-H. Moon, J. Y. Hyun, K. H. Kim, D. Lee, J.-S. Lee, W. B. Im, A zero-thermal-quenching phosphor. *Nat. Mater.* **16**, 543–550 (2017).
12. H. Ding, J. Li, G. Xie, G. Lin, R. Chen, Z. Peng, C. Yang, B. Wang, J. Sun, C. Wang, An AIEgen-based 3D covalent organic framework for white light-emitting diodes. *Nat. Commun.* **9**, 5234 (2018).
13. C.-Y. Sun, X.-L. Wang, X. Zhang, C. Qin, P. Li, Z.-M. Su, D.-X. Zhu, G.-G. Shan, K.-Z. Shao, H. Wu, J. Li, Efficient and tunable white-light emission of metal-organic frameworks by iridium-complex encapsulation. *Nat. Commun.* **4**, 2717 (2013).
14. N. Hendler, B. Belgorodsky, E. D. Mentovich, M. Gozin, S. Richter, Efficient separation of dyes by mucin: Toward bioinspired white-luminescent devices. *Adv. Mater.* **23**, 4261–4264 (2011).
15. Z. Wang, F. Yuan, X. Li, Y. Li, H. Zhong, L. Fan, S. Yang, 53% efficient red emissive carbon quantum dots for high color rendering and stable warm white-light-emitting diodes. *Adv. Mater.* **29**, 1702910 (2017).
16. S. Qu, D. Zhou, D. Li, W. Ji, P. Jing, D. Han, L. Liu, H. Zeng, D. Shen, Toward efficient orange emissive carbon nanodots through conjugated sp^2-domain controlling and surface charges engineering. *Adv. Mater.* **28**, 3516–3521 (2016).
17. H. Ding, S.-B. Yu, J.-S. Wei, H.-M. Xiong, Full-color light-emitting carbon dots with a surface-state-controlled luminescence mechanism. *ACS Nano* **10**, 484–491 (2016).
18. Y. Yan, J. Chen, N. Li, J. Tian, K. Li, J. Jiang, J. Liu, Q. Tian, P. Chen, Systematic bandgap engineering of graphene quantum dots and applications for photocatalytic water splitting and CO_2 reduction. *ACS Nano* **12**, 3523–3532 (2018).
19. S. Yang, W. Li, C. Ye, G. Wang, H. Tian, C. Zhu, P. He, G. Ding, X. Xie, Y. Liu, Y. Lifshitz, S.-T. Lee, Z. Kang, M. Jiang, C_3N—A 2D crystalline, hole-free, tunable-narrow-bandgap semiconductor with ferromagnetic properties. *Adv. Mater.* **29**, 1605625 (2017).
20. N. Gong, X. Ma, X. Ye, Q. Zhou, X. Chen, X. Tan, S. Yao, S. Huo, T. Zhang, S. Chen, X. Teng, X. Hu, J. Yu, Y. Gan, H. Jiang, J. Li, X.-J. Liang, Carbon-dot-supported atomically dispersed gold as a mitochondrial oxidative stress amplifier for cancer treatment. *Nat. Nanotechnol.* **14**, 379–387 (2019).
21. S. D. Pritzl, F. Pschunder, F. Ehrat, S. Bhattacharyya, T. Lohmüller, M. A. Huergo, J. Feldmann, Trans-membrane fluorescence enhancement by carbon dots: Ionic interactions and energy transfer. *Nano Lett.* **19**, 3886–3891 (2019).
22. P. Huang, J. Lin, X. Wang, Z. Wang, C. Zhang, M. He, K. Wang, F. Chen, Z. Li, G. Shen, D. Cui, X. Chen, Light-triggered theranostics based on photosensitizer-conjugated carbon dots for simultaneous enhanced-fluorescence imaging and photodynamic therapy. *Adv. Mater.* **24**, 5104–5110 (2012).
23. K. Holá, M. Sudolská, S. Kalytchuk, D. Nachtigallová, A. L. Rogach, M. Otyepka, R. Zbořil, Graphitic nitrogen triggers red fluorescence in carbon dots. *ACS Nano* **11**, 12402–12410 (2017).
24. X. Geng, Y. Sun, Z. Li, R. Yang, Y. Zhao, Y. Guo, J. Xu, F. Li, Y. Wang, S. Lu, L. Qu, Retrosynthesis of tunable fluorescent carbon dots for precise long-term mitochondrial tracking. *Small* **15**, e1901517 (2019).
25. W. Li, W. Zhou, Z. Zhou, H. Zhang, X. Zhang, J. Zhuang, Y. Liu, B. Lei, C. Hu, A universal strategy for activating the multicolor room-temperature afterglow of carbon dots in a boric acid matrix. *Angew. Chem. Int. Ed.* **58**, 7278–7283 (2019).
26. S. Zhu, Q. Meng, L. Wang, J. Zhang, Y. Song, H. Jin, K. Zhang, H. Sun, H. Wang, B. Yang, Highly photoluminescent carbon dots for multicolor patterning, sensors, and bioimaging. *Angew. Chem. Int. Ed.* **52**, 3953–3957 (2013).
27. K. Jiang, S. Sun, L. Zhang, Y. Lu, A. Wu, C. Cai, H. Lin, Red, green, and blue luminescence by carbon dots: Full-color emission tuning and multicolor cellular imaging. *Angew. Chem. Int. Ed.* **54**, 5360–5363 (2015).
28. L. Wang, B. Wu, W. Li, Z. Li, J. Zhan, B. Geng, S. Wang, D. Pan, M. Wu, Industrial production of ultra-stable sulfonated graphene quantum dots for Golgi apparatus imaging. *J. Mater. Chem. B* **5**, 5355–5361 (2017).
29. B. Zhang, Y. Liu, M. Ren, W. Li, X. Zhang, R. Vajtai, P. M. Ajayan, J. M. Tour, L. Wang, Sustainable synthesis of bright green fluorescent nitrogen-doped carbon quantum dots from alkali lignin. *ChemSusChem* **12**, 4202–4210 (2019).
30. Y. Han, M. Li, J. Lai, W. Li, Y. Liu, L. Yin, L. Yang, X. Xue, R. Vajtai, P. M. Ajayan, L. Wang, Rational design of oxygen-enriched carbon dots with efficient room-temperature phosphorescent properties and high-tech security protection application. *ACS Sustain. Chem. Eng.* **7**, 19918–19924 (2019).
31. X. Miao, D. Qu, D. Yang, B. Nie, Y. Zhao, H. Fan, Z. Sun, Synthesis of carbon dots with multiple color emission by controlled graphitization and surface functionalization. *Adv. Mater.* **30**, 1704740 (2018).
32. F. Yuan, T. Yuan, L. Sui, Z. Wang, Z. Xi, Y. Li, X. Li, L. Fan, Z. Tan, A. Chen, M. Jin, S. Yang, Engineering triangular carbon quantum dots with unprecedented narrow bandwidth emission for multicolored LEDs. *Nat. Commun.* **9**, 2249 (2018).
33. Z. Liu, H. Pei, L. Zhang, Y. Tian, Mitochondria-targeted DNA nanoprobe for real-time imaging and simultaneous quantification of Ca^{2+} and pH in neurons. *ACS Nano* **12**, 12357–12368 (2018).
34. J. Shao, S. Zhu, H. Liu, Y. Song, S. Tao, B. Yang, Full-color emission polymer carbon dots with quench-resistant solid-state fluorescence. *Adv. Sci.* **4**, 1700395 (2017).
35. Z. Tian, X. Zhang, D. Li, D. Zhou, P. Jing, D. Shen, S. Qu, R. Zboril, A. L. Rogach, Full-color inorganic carbon dot phosphors for white-light-emitting diodes. *Adv. Opt. Mater.* **5**, 1700416 (2017).
36. Y. Li, Y. Zhao, H. Cheng, Y. Hu, G. Shi, L. Dai, L. Qu, Nitrogen-doped graphene quantum dots with oxygen-rich functional groups. *J. Am. Chem. Soc.* **134**, 15–18 (2012).
37. L. Wang, Y. Wang, T. Xu, H. Liao, C. Yao, Y. Liu, Z. Li, Z. Chen, D. Pan, L. Sun, M. Wu, Gram-scale synthesis of single-crystalline graphene quantum dots with superior optical properties. *Nat. Commun.* **5**, 5357 (2014).
38. Z. Luo, G. Qi, K. Chen, M. Zou, L. Yuwen, X. Zhang, W. Huang, L. Wang, Microwave-assisted preparation of white fluorescent graphene quantum dots as a novel phosphor for enhanced white-light-emitting diodes. *Adv. Funct. Mater.* **26**, 2739–2744 (2016).
39. F. Arcudi, L. Đorđević, M. Prato, Rationally designed carbon nanodots towards pure white-light emission. *Angew. Chem. Int. Ed.* **56**, 4170–4173 (2017).
40. T. Meng, T. Yuan, X. Li, Y. Li, L. Fan, S. Yang, Ultrabroad-band, red sufficient, solid white emission from carbon quantum dot aggregation for single component warm white light emitting diodes with a 91 high color rendering index. *Chem. Commun.* **55**, 6531–6534 (2019).

Acknowledgments: We thank the Laboratory for Microstructures of Shanghai University. **Funding:** This work was supported by the National Natural Science Foundation of China (nos. 21671129, 21901154, 21671131, 51605272, 11875185, and 41430644), the Shanghai Sailing Program (no. 16YF1404400), and the Program for Changjiang Scholars and Innovative Research Team in University (no. IRT_17R71). **Author contributions:** L.W. and M.W. conceived the idea and supervised the project. P.M.A. and R.V. provided important suggestions, supervised parts of the project, and improved the manuscript. L.W. and W.L. conducted most of the experiments regarding the CQD fabrication and characterization. Y.L., H.G., J.L., Y.H., G.L., and M.L. supported the optical performance. L.Y. and J.Z. helped with WLED part experiment. L.W. wrote the manuscript. All authors analyzed and discussed the experimental data and drafted the manuscript. **Competing interests:** The authors declare that they have no competing interests. **Data and materials availability:** All data needed to evaluate the conclusions in the paper are present in the paper and/or the Supplementary Materials. Additional data related to this paper may be requested from the authors.

Submitted 11 March 2020
Accepted 19 August 2020
Published 2 October 2020
10.1126/sciadv.abb6772

Citation: L. Wang, W. Li, L. Yin, Y. Liu, H. Guo, J. Lai, Y. Han, G. Li, M. Li, J. Zhang, R. Vajtai, P. M. Ajayan, M. Wu, Full-color fluorescent carbon quantum dots. *Sci. Adv.* **6**, eabb6772 (2020).

Science Advances

Full-color fluorescent carbon quantum dots

Liang Wang, Weitao Li, Luqiao Yin, Yijian Liu, Huazhang Guo, Jiawei Lai, Yu Han, Gao Li, Ming Li, Jianhua Zhang, Robert Vajtai, Pulickel M. Ajayan and Minghong Wu

Sci Adv **6** (40), eabb6772.
DOI: 10.1126/sciadv.abb6772

Science Advances (ISSN 2375-2548) is published by the American Association for the Advancement of Science, 1200 New York Avenue NW, Washington, DC 20005. The title *Science Advances* is a registered trademark of AAAS.